SUPPLEMENTARY MATERIALS

SUPPLEMENTARY METHODS

Reagents

Recombinant human P-selectin (CD62P)-Fc chimera and recombinant human ICAM-1 (CD54)-Fc chimera were obtained from R&D Systems (Minneapolis, MN). Recombinant human CXCL8/interleukin-8 (IL-8) was obtained from Peprotech Inc. (Rocky Hill, NJ). Alexa Fluor 647 (AF647) conjugated mouse anti-human CD16 mAb (clone 3G8; $IgG_1\kappa$), fluorescein isothiocyanate (FITC) conjugated mouse anti-human CD49b mAb (clone AK-7; $IgG_1\kappa$), function blocking NA/LE mouse anti-human CD11b (Mac-1) mAb (clone ICFR44; $IgG_1\kappa$), purified NA/LE mouse $IgG_1\kappa$ isotype control (clone 107.3), Brilliant Violet 421 (BV421) mouse anti-human CD62P (clone AK-4), FITC mouse IgG1 κ (clone MOPC-21), phycoerythrin (PE) mouse IgG1 κ (clone MOPC-21), Violet 450 (V450) rat-anti mouse CD49b mAb (clone DX5), FITC rat anti-mouse Ly-6G mAb (clone 1A8), FITC rat $IgG_{2a,\kappa}$ isotype control mAb (clone R35-95), PE rat anti-mouse CD41 mAb (clone MWReg30), BV421 rat anti-mouse CD11b mAb (clone M1/70), BV421 rat $IgG_{2b,\kappa}$ isotype control mAb (clone R35-38) and purified mouse anti-human CD162 (clone KPL-1) were purchased from BD Biosciences (San Jose, CA). Alexa Fluor 546 (AF546) rat anti-mouse Ly-6G mAb (clone 1A8) and FITC rat anti-mouse TER-119 mAb (clone TER-119) were purchased from BioLegend (San Diego, CA). PE rat $IgG_{1,\kappa}$ isotype control mAb (clone eBRG1) was purchased from eBioscience Inc. (San Diego, CA). FITC dextran (MW 70,000) was purchased from Molecular Probes Inc. (Eugene, OR). Function blocking mouse anti-human CD62P (P-selectin) mAb (clone G1/G14; $IgG_{1\kappa}$) was purchased from Ancell Corp. (Bayport, MN). Toll like receptor-4 (TLR4) inhibitor TAK242 (CLI-095) was purchased from InvivoGen (San Diego, CA) and solubilized in Intralipid (20% emulsion) purchased from Sigma-

Aldrich (St. Louis, MO). Function blocking mAbs rat IgG_1 against mouse P-selectin (clone RB40.34) and rat IgG_{2b} against mouse Fc-receptor (clone 2.4G2) were prepared from a hybridoma culture supernatant at the Lymphocyte Culture Center, University of Virginia. Dietmar Vestweber, MD at Max Planck Institute for Molecular Biomedicine-Munster provided the hybridoma culture used in generating the anti-mouse-P-selectin mAb (RB40.34). The Fab preparation kit (catalog no. 44985) and AF647 conjugated phalloidin were purchased from Thermo Fischer Scientific (Waltham, MA). Evans blue, thiazole orange, gram negative bacterial lipopolysaccharide (LPS) from *Escherichia coli 0111:B4* (*E. coli*) and apyrase were purchased from Sigma-Aldrich. Prostaglandin I_2 (PGI_2) was purchased from EMD Millipore (Billerica, MA). The mouse lung dissociation kit (catalog no. 130-095-927) was purchased from Miltenyi Biotec (Bergisch Gladbach, Germany). Cy3 conjugated AffiniPure donkey anti-mouse IgG (H+L) polyclonal (715-165-151**)** was purchased from Jackson Immuno Research Laboratories, Inc (West Grove, PA). Ketamine HCl (100 mg/ml) and atropine sulfate (0.54 mg/ml) were purchased from Henry Schein Animal Health (Dublin, OH) and xylazine (20 mg/ml) was purchased from LLOYD Laboratories (Shenandoah, IA). Mouse anti-human CD42b mAb (clone VM16d) was purchased from Abcam (San Francisco, CA).

Mice

BERK sickle cell disease (SCD) and control mouse phenotypes were confirmed in-house. Circulating blood counts (CBCs) and hemoglobin (Hb) levels were determined using the Hemavet® HV950 (Drew Scientific, Miami Lakes, FL). Blood was labeled with thiazole orange and the percent of reticulocytes was quantified by flow cytometry using the BD LSR Fortessa

flow cytometer. Hb electrophoresis was performed using precast gels (hydragel 15 Hb, catalog no. 4126) and the HYDRASYS system from Sebia Electrophoresis (Norcross, GA).

Quantitative fluorescence intravital lung microscopy

Recently, we introduced multi-photon-excitation (MPE) enabled quantitative fluorescence intravital lung microscopy (qFILM) in live SCD mice (1). qFILM is inspired by the stabilized imaging window approach introduced by Looney et al (2). In the current study, qFILM was used to assess the LPS-induced cellular events that promulgate pulmonary vaso-occlusion in live control and SCD mice. The microscopic setup used in qFILM has been described previously in detail (1). qFILM of the mouse pulmonary microcirculation was performed using a Nikon A1R MP configured with the Nikon Ni-E upright motorized microscope (Nikon Instruments; Tokyo, Japan). Two dimensional time series of qFILM images were acquired with NIS-Elements software using a prechirped Chameleon Laser Vision (Coherent; Santa Clara, CA) emitting an excitation wavelength of 850 nm, an APO LWD 25x water immersion objective with 1.1 NA, a high speed resonant scanning mode capable of acquisition at 512 x 512 resolution with 2x line averaging and bi-directional scanning (14.83 frames per second) and four GaAsP NDD detectors. The four detectors collected fluorescent light transmitted through 450/20 nm (detector 1; blue channel), 525/50 nm (detector 2; green channel), 576/26 nm (detector 3; red channel) and 685/70 nm (detector 4; far red channel) band pass filters. In this study, we used detector 1 for V450, detector 2 for FITC, detector 3 for AF546 and detector 4 for Evans blue. The position of the microscope stage was selected in the *z* and *x-y* planes through a Nano-Drive (Mad City Labs Inc.; Madison, WI) and a control pad (Prior Scientific Inc.; Rockland, MA), respectively.

qFILM observations made in the current study were limited by the size of the imaging window (~20 mm^2) (1). Also qFILM observations were primarily made in the lower portion of the left lung, as this lobe is the easiest to visualize and most importantly, radiographic and histopathological studies have repeatedly shown that the lower lobes are the most affected regions of the lung in SCD patients (3, 4). However, to circumvent this limitation, flow cytometry was also used in the current study to assess the presence of neutrophil-platelet aggregates in digested whole lung cell suspensions from control and SCD mice. In support of qFILM findings, SCD mice were found to have greater neutrophil-platelet aggregates in whole lung cell suspensions compared to control mice after IV saline or LPS administration. We observed that the distribution of pulmonary vaso-occlusions was heterogeneous; vaso-occlusions were present in some areas of the lung and absent in others. To ensure an accurate estimation of the vaso-occlusive burden, multiple FOVs per mouse (5-10) were randomly selected and imaged using qFILM over multiple mice for each test group.

Experimental design of qFILM studies

The pulmonary microcirculation was labeled with Evans blue or FITC dextran. Neutrophils, platelets and erythrocytes were labeled in vivo with fluorescent antibodies including AF546-conjugated Ly-6G mAb, V450-conjugated CD49b mAb and FITC-conjugated TER-119 mAb, respectively. As the in vivo staining of CD41 with fluorescent mAbs can compromise platelet aggregation in mouse models of inflammation, Jenne *et al* (5) have validated that CD49b is a better and more reliable marker than CD41 for intravital fluorescence visualization of platelets in the mouse microvasculature. Although CD49b is expressed on both platelets and NK cells, NK cells are extremely rare in blood compared to platelets and do not interfere with the visualization

of platelets (5). Also, the dose of 12 µg/mouse anti-Ly-6G mAb used in the current study has been established by previous studies to be optimum for intravital visualization of neutrophils without compromising neutrophil recruitment (6, 7).

A single 2D plane in the *z*-direction was selected and multiple field of views (FOV ~260 µm x 260 µm at 0.5 µm per pixel resolution) were acquired for each mouse over a total observation period of 30 minutes followed by euthanization of mice by an overdose of anesthesia. Time series of qFILM images were recorded for each FOV over a period ranging from 30 seconds to 2 minutes. During image acquisition, physiological parameters of the mice such as blood pressure, heart rate, blood oxygen tension, pulse distention, breath distention and breath rate were monitored continuously as previously described (1).

qFILM image processing and analysis

Time series of qFILM 2D images were processed in Nikon's NIS-Elements software. Image subtraction was used to remove some of the autofluorescence from all channels and minimize the bleed through from the vessel channel (green channel for FITC dextran or far red channel for Evans blue) into the neutrophil channel (red channel for AF546). The signal-to-noise ratio was improved through application of a median filter and a noise-reduction algorithm. Signal contrast was further enhanced by adjusting the maxima and minima of the intensity histogram associated with each channel. Some channels were pseudo-colored as noted in the figure legends. All image processing operations were performed uniformly on every image frame over the whole FOV. Chosen FOVs were then cropped to show magnified versions of selected pulmonary vaso-occlusions. For a small number of videos with more prominent lung movement, the peak

inspiratory and/or expiratory frame in each breathing cycle was removed to decrease *z* drift in the time series.

Pulmonary arterioles were analyzed for the quantitative assessment of vaso-occlusions. Arterioles were distinguished from venules by the direction of flow. In arterioles, the flow is directed down a large vessel into the smaller daughter arterioles or the pulmonary capillaries; whereas in venules, the flow is directed from the pulmonary capillaries or smaller vessels into a larger vessel. QFILM revealed that the occurrence of pulmonary vaso-occlusions was heterogeneous; vaso-occlusions were present in some areas of the lung and absent in others within the same mouse. Therefore, pulmonary vaso-occlusions were quantified for randomly selected multiple (5-10) FOVs over several mice in each group (n=3 to 5 mice) to exclude a possibility of bias. Only the first 30 seconds of each qFILM time series was analyzed. Pulmonary vaso-occlusions were defined as cellular aggregates blocking the blood flow within the pre-capillary branches of arterioles (see Figure 1E).

The following criteria were used to define pulmonary vaso-occlusions:

1) We (1) and others (8) have shown that neutrophils, being larger in diameter than most pulmonary capillaries, deform into an ellipsoid filling the entire lumen of the pulmonary capillaries. Therefore, a fraction of pulmonary capillaries are always occluded with these neutrophils which are slowly transiting through the pulmonary capillary network. The population of resident neutrophils referred to as the “marginated pool” has been shown to exist even in healthy lungs. Thus only vaso-occlusions extending from the capillaries into the arteriolar

branches were quantified (Figure 1E), whereas vaso-occlusions localized in nearby capillaries were not considered.

2) Only cellular aggregates completely filling the diameter of the arteriolar branches were quantified; however, cellular adhesion to the arteriolar wall and partial blockage of the lumen diameter was not considered as a pulmonary vaso-occlusion, as the partial blockage did not result in complete stasis.

3) Arteriolar branches had to be occluded by more than 2 neutrophils to be considered as a pulmonary vaso-occlusion. The average diameter of a neutrophil is larger in size than the diameter of pulmonary capillaries, thus requiring that the neutrophil actively deform to fit through the capillaries. Therefore, a small vaso-occlusion containing 1 or 2 neutrophils can just be the result of normal neutrophil trafficking throughout the lung and such an event was not quantified in this analysis.

4) Multiple vaso-occlusions per FOV were quantified when several separate arteriolar branches were blocked by cellular aggregates.

The average number of pulmonary vaso-occlusions per FOV, the percent of FOVs with pulmonary vaso-occlusions, the area of pulmonary vaso-occlusions and the cellular composition of pulmonary vaso-occlusions were quantified. For each test group, the total number of vaso-occlusions observed were counted across all mice and divided by the total number of FOVs to determine the average number of pulmonary vaso-occlusions per FOV. The area of pulmonary vaso-occlusions was measured using an ellipsoidal tracing tool in NIS-Elements (refer to illustration in Figure 1E). Pulmonary vaso-occlusions were classified into three categories based on their cellular composition (Figure 1E-H): 1) predominantly neutrophils with few platelets

adhered to neutrophils (neutrophil vaso-occlusion); 2) predominantly platelets with few neutrophils attached to platelets (platelet vaso-occlusion) and 3) predominantly other cell types with few neutrophils and/or platelets (other vaso-occlusion). The diameter of arterioles shown in each figure was determined using a line tracing tool in NIS-Elements. When multiple FOVs are shown for a given test condition, the average arteriole diameter ± standard deviation is mentioned in the figure legends.

Flow cytometry of whole lung

The presence of neutrophil-platelet aggregates in whole digested lung was assessed using flow cytometry (9). Mice were injected with IV saline or 0.1 µg/kg IV LPS via tail vein 2 to 2.5 hours before euthanasia by CO_2 overdose. Immediately following euthanasia, whole blood was collected into a heparinized syringe via cardiac puncture. The lungs were excised, rinsed in phosphate buffered saline (PBS without Ca^{2+} and Mg^{2+}; pH 7.4), and digested to form a cell suspension according to the mouse lung dissociation kit protocol provided by Miltenyi Biotec. Whole lung samples for flow cytometry were prepared by incubating the cell suspension with red blood cell lysis buffer (eBioscience) followed by washing with Tyrode's buffer (134 mM NaCl, 12 mM $NaHCO_3$, 2.9 mM KCl, 0.34 mM Na_2HPO_4, 1 mM $MgCl_2$, 10 mM HEPES, 1% BSA and 0.1% sodium azide) at 300G for 5 min (22˚C) in a centrifuge. Cells were incubated in Tyrode's buffer supplemented with 7 units/ml apyrase and 0.5 µM PGI_2 for 30 minutes on ice with the following antibodies: rat IgG_{2b} against mouse Fc-receptor, FITC rat anti-mouse Ly-6G mAb, PE rat anti-mouse CD41 mAb, BV421 rat anti-mouse CD11b mAb and the appropriate isotype control mAbs listed in the Reagents section. Cells were washed, resuspended in supplemented Tyrode's buffer and analyzed on a BD LSR Fortessa flow cytometer using the 405 nm (BV421)

and 488 nm (FITC, PE) lasers. Compensation was performed prior to sample acquisition with the anti-rat and anti-hamster IgGκ/negative control compensation beads set from BD Biosciences. A gate was created around granulocytes on the side scatter vs. forward scatter plot and 100,000 to 150,000 events were recorded within this gate for each sample (Figure S8). Analysis was performed using FlowJo software v10 (Tree Star Inc., Ashland, OR). Neutrophils were defined as $FSC^{hi}/SSC^{hi}/Ly\text{-}6G^{+}/CD11b^{+}$ and neutrophil-platelet aggregates were defined as $Ly\text{-}6G^{+}/CD11b^{+}/CD41^{+}$.

Quantitative microfluidic fluorescence microscopy

Neutrophils are the most abundant leukocytes (70-80%) in human blood and are defined as dual positive for CD66b and CD16 ($CD66b^{+}/CD16^{+}$) (10, 11). We have shown previously using flow cytometry that 94% of $CD16^{+}$ cells in human blood are neutrophils ($CD16^{+}/CD66b^{+}$) (12). We (12) and others (7) have also shown that CD16 can be used as a marker to identify human neutrophils by fluorescence microscopy. Neutrophils and platelets were labeled in vitro in human blood samples with AF647-conjugated CD16 and FITC-conjugated CD49b mAbs, respectively.

The two-stage imaging strategy used in quantitative microfluidic fluorescence microscopy (qMFM) is a combination of quantitative dynamic footprinting (qDF-stage-1) and epifluorescence microscopy (stage-2). qDF is an adaptation of total internal reflection fluorescence (TIRF) microscopy that allows visualization of the footprint of rolling, arresting and crawling neutrophils on a glass substrate coated with adhesion molecules (13, 14). qMFM images were recorded using a Nikon Eclipse-Ti inverted microscope with a TIRF photo-activation unit (NIKON, Melville, NY), a Zyla-5.5 sCMOS scientific camera (5.5 Megapixel

resolution; maximum frame rate 100 s^{-1}; ANDOR, South Windsor, CT) and a motorized Nikon Intensilight CHGFIE fiber illuminator as an epifluorescence source. The microscope was equipped with 405 nm, 488 nm, 560 nm and 640 nm lasers housed in a MLC Monolithic Laser combiner launch (Agilent Technologies, Santa Clara, CA). Observations were made using a CFI Apochromat TIRF 60x oil objective (NA 1.49). The laser, camera, filters and other microscope functions were controlled using NIS-Elements software (Nikon) installed on a PC. NIS-Elements allowed sequential capture of the green (FITC) and far red channels (AF647) through a quad-filter by switching between the two lasers at a minimum interval of 10 ms. In the current study, qMFM observations were acquired at a frame rate of 10 frames per second.

Experimental design of qMFM studies

Antibody blocking studies were performed using a strategy that allowed inhibition of platelet-neutrophil interactions without causing detachment of arrested neutrophils. The blood was perfused in the microfluidic micro-channels for 2 min, which allowed neutrophils to roll, arrest firmly and then interact with circulating platelets. Once the neutrophils were firmly arrested, platelet-neutrophil interactions were recorded using qMFM for the next 2 min. After 2 min of qMFM observations, the flow was stopped momentarily and function blocking anti-CD62P and/or anti-CD11b mAbs (1:100 dilution) or isotype control IgG_1 Ab (1:100 dilution) was added to the blood in the reservoir. The flow was resumed and the effect on platelet-neutrophil interactions was assessed over the next 2 min. Once neutrophils are arrested, P-selectin is not required to maintain the firm adhesion of arrested neutrophils to the ICAM-1 presenting substrate (15) and thus, blocking P-selectin post firm arrest should not result in the detachment of arrested neutrophils. CD11a/CD18 (LFA-1) as well as CD11b/CD18 (Mac-1), the two major

neutrophil β2-integrins have an overlapping role in mediating neutrophil arrest and crawling on an ICAM-1 presenting substrate (15). Therefore, blocking Mac-1 should not result in detachment of firmly arrested neutrophils. To validate this, we analyzed the qMFM data and found no difference in the number of arrested neutrophils pre and post addition of the cocktail of anti-CD62P and anti-CD11b mAbs (Figure 4E).

LPS treatment was conducted by incubating blood for 10 min with LPS at room temperature (22˚C) followed by the addition of fluorescent anti-CD16 and anti-CD49b Abs to stain neutrophils and platelets, respectively and perfusion of the blood through the micro-channels. Platelet-neutrophil interactions were visualized using both steps of qMFM as described previously (12). Function blocking with anti-CD62P and/or anti-CD11b mAbs, anti-CD42b mAb, anti-CD162 mAb (1:100 dilution), or isotype control IgG_1 Ab (1:100 dilution) post LPS incubation was performed as described above. Experiments testing the role of Toll-Like-Receptor-4 (TLR-4) inhibition were done by adding TAK-242+intralipid (50 μg/mL) into the blood and incubating for 5 min. After 5 min, LPS was added to the blood followed by incubation for 10 min at room temperature (22˚C) and perfusion through the micro-channels.

qMFM image processing and analysis

Image processing and analysis of qMFM images has been described previously (12). Time series of qMFM images were analyzed to estimate the number of platelet-neutrophil interactions per 2 minutes, the number of neutrophils arresting per minute, the number of platelet-neutrophil interactions per arrested neutrophil and the lifetime of platelet-neutrophil interactions in a FOV of area ~14,520 μm^2. Platelet interactions per neutrophil were determined by randomly selecting

10 neutrophils per FOV, observing each individual neutrophil over a 2 minute time period and counting the total number of platelets interacting with these neutrophils. qMFM data was acquired over ~2 FOVs in every experiment and a mean value for each parameter per FOV was estimated based on at least three independent experiments for each condition. Lifetimes of platelet-neutrophil interactions were determined by randomly selecting ~45 individual platelets throughout the data set and measuring the length of their interactions with arrested neutrophils.

Scanning electron microscopy

Neutrophil-platelet aggregates in control and SCD human blood were perfusion-fixed and analyzed with a scanning electron microscope as described previously (12). Freshly collected whole blood was perfused through microfluidic micro-channels coated with P-selectin, ICAM-1 and IL-8. Neutrophils were allowed to roll and arrest on the coverslip and interact with freely flowing platelets. Following a 3-min perfusion at a wall shear stress of 6 dynes cm^{-2}, a cocktail of 4% paraformaldehyde and 2.5% glutaraldehyde was perfused through the micro-channels at the same wall shear stress to fix the adhered/interacting cells in the presence of flow. Coverslips were detached from the microfluidic chip and visualized using a Field Emission Scanning Electron Microscope (JEOL JSM 6335F) as described previously (12). Scanning electron micrographs were pseudo-colored (as shown in Figure 3C) using Adobe Photoshop (Adobe Inc.). Images were duplicated and colored using the color table with corresponding colors to create multiple colorized images. Structures were then selected using the pencil tool and copy-pasted on top of each other to create a multicolor SEM micrograph. Alignment of the structures was done using the move tool in Adobe Photoshop.

Structured illumination microscopy

BV421 conjugated anti-human CD62P mAb or isotype control mouse IgG1κ was added to the blood and cells were fixed under flow using the same protocol used for scanning electron microscopy. Coverslips were washed with PBS (without Ca^{2+} and Mg^{2+}) and permeabilized with 0.1% Triton X-100 in PBS for 15 minutes. Cover slips were washed three times with PBS followed by three washes with PBS containing 0.5% BSA. Cells were blocked with PBS containing 2% BSA for 45 minutes and then washed five times with PBS containing 0.5% BSA. Coverslips were incubated with AF647-phalloidin to stain F-actin and a Cy3 conjugated donkey anti-mouse IgG to enhance the signal of the anti-CD62P mAb for 45 minutes. Finally, coverslips were washed three times with PBS, mounted to a glass slide with Gelvatol, and stored at 4ºC in the dark until imaging. Images were processed using NIS-Elements software. No fluorescence was observed in samples stained with the isotype mouse IgG1κ Ab.

References

1. Bennewitz MF, Watkins SC, and Sundd P. Quantitative intravital two-photon excitation microscopy reveals absence of pulmonary vaso-occlusion in unchallenged Sickle Cell Disease mice. *IntraVital.* 2014;3(1):e29748.
2. Looney MR, Thornton EE, Sen D, Lamm WJ, Glenny RW, and Krummel MF. Stabilized imaging of immune surveillance in the mouse lung. *Nat Methods.* 2011;8(1):91-6.
3. Mekontso Dessap A, Deux JF, Abidi N, Lavenu-Bombled C, Melica G, Renaud B, Godeau B, Adnot S, Brochard L, Brun-Buisson C, et al. Pulmonary artery thrombosis during acute chest syndrome in sickle cell disease. *American journal of respiratory and critical care medicine.* 2011;184(9):1022-9.
4. Anea CB, Lyon M, Lee IA, Gonzales JN, Adeyemi A, Falls G, Kutlar A, and Brittain JE. Pulmonary platelet thrombi and vascular pathology in acute chest syndrome in patients with sickle cell disease. *American journal of hematology.* 2016;91(2):173-8.
5. Jenne CN, Wong CH, Petri B, and Kubes P. The use of spinning-disk confocal microscopy for the intravital analysis of platelet dynamics in response to systemic and local inflammation. *PloS one.* 2011;6(9):e25109.
6. Yipp BG, and Kubes P. Antibodies against neutrophil LY6G do not inhibit leukocyte recruitment in mice in vivo. *Blood.* 2013;121(1):241-2.
7. Yipp BG, Petri B, Salina D, Jenne CN, Scott BN, Zbytnuik LD, Pittman K, Asaduzzaman M, Wu K, Meijndert HC, et al. Infection-induced NETosis is a dynamic process involving neutrophil multitasking in vivo. *Nat Med.* 2012;18(9):1386-93.
8. Doerschuk CM. Mechanisms of leukocyte sequestration in inflamed lungs. *Microcirculation.* 2001;8(2):71-88.

9. Ortiz-Munoz G, Mallavia B, Bins A, Headley M, Krummel MF, and Looney MR. Aspirin-triggered 15-epi-lipoxin A4 regulates neutrophil-platelet aggregation and attenuates acute lung injury in mice. *Blood.* 2014;124(17):2625-34.

10. Nauseef WM, and Borregaard N. Neutrophils at work. *Nature immunology.* 2014;15(7):602-11.

11. Dominical VM, Samsel L, Nichols JS, Costa FF, McCoy JP, Jr., Conran N, and Kato GJ. Prominent role of platelets in the formation of circulating neutrophil-red cell heterocellular aggregates in sickle cell anemia. *Haematologica.* 2014;99(11):e214-7.

12. Jimenez MA, Tutuncuoglu E, Barge S, Novelli EM, and Sundd P. Quantitative microfluidic fluorescence microscopy to study vaso-occlusion in sickle cell disease. *Haematologica.* 2015;100(10):e390-3.

13. Sundd P, Gutierrez E, Pospieszalska MK, Zhang H, Groisman A, and Ley K. Quantitative dynamic footprinting microscopy reveals mechanisms of neutrophil rolling. *Nature Methods.* 2010;7(10):821-4.

14. Sundd P, Gutierrez E, Koltsova EK, Kuwano Y, Fukuda S, Pospieszalska MK, Groisman A, and Ley K. 'Slings' enable neutrophil rolling at high shear. *Nature.* 2012;488(7411):399-403.

15. Kolaczkowska E, and Kubes P. Neutrophil recruitment and function in health and inflammation. *Nature reviews Immunology.* 2013;13(3):159-75.

SUPPLEMENTARY FIGURES

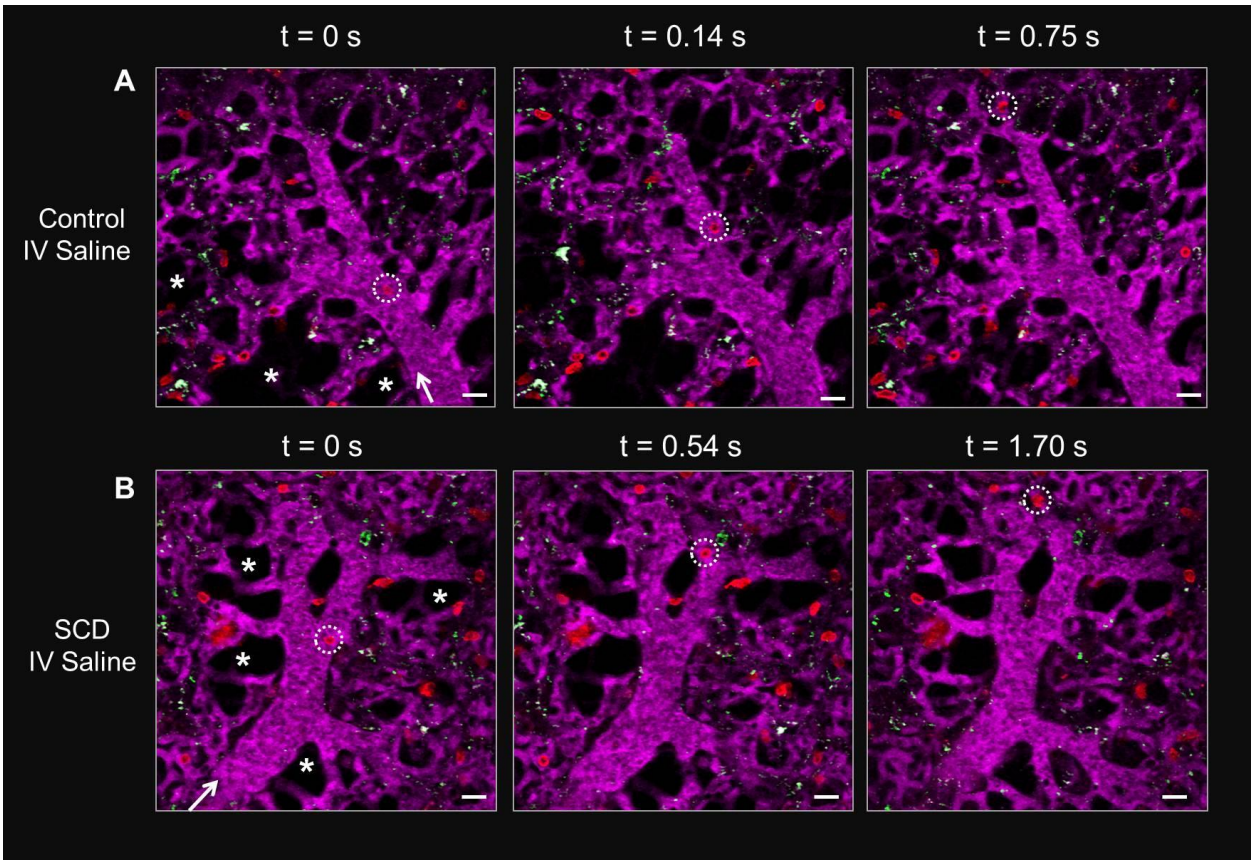

Figure S1. Neutrophil trafficking is not impeded in the lungs of control and SCD mice following IV saline. Control and sickle cell disease (SCD) mice were injected intravenously (IV) with saline and pulmonary arterioles were imaged using quantitative fluorescence intravital lung microscopy (qFILM) to evaluate neutrophil-platelet interactions. qFILM images are shown of the same field of view (FOV) at 3 different time points to demonstrate that neutrophil-platelet interactions occur rarely in the large pulmonary vessels after IV saline in both (**A**) control and (**B**) SCD mice. Dotted circles highlight neutrophils rapidly transiting through the pulmonary arteriolar branches, just prior to entering the capillaries. Platelets (green) and neutrophils (red) were stained by IV administration of V450-CD49b mAb and AF546-Ly6G mAb, respectively. The pulmonary microcirculation including a feeding arteriole and surrounding capillaries

(purple) were visualized by IV administration of FITC-dextran. Pseudo-coloring was used for platelets and pulmonary vessels to enhance contrast. * denote the alveoli. White arrows mark the direction of blood flow within the feeding arterioles. The times displayed are relative to the selected video frames. The diameters of the arterioles shown in **A** and **B** are 33 μm and 38 μm, respectively. Scale bars are 20 μm. These images are selected from 1 representative control and SCD mouse administered with IV saline (total n = 3 control and n = 3 SCD mice; control = 23 FOVs; SCD = 29 FOVs). The complete time series are included in Movies S1 and S2.

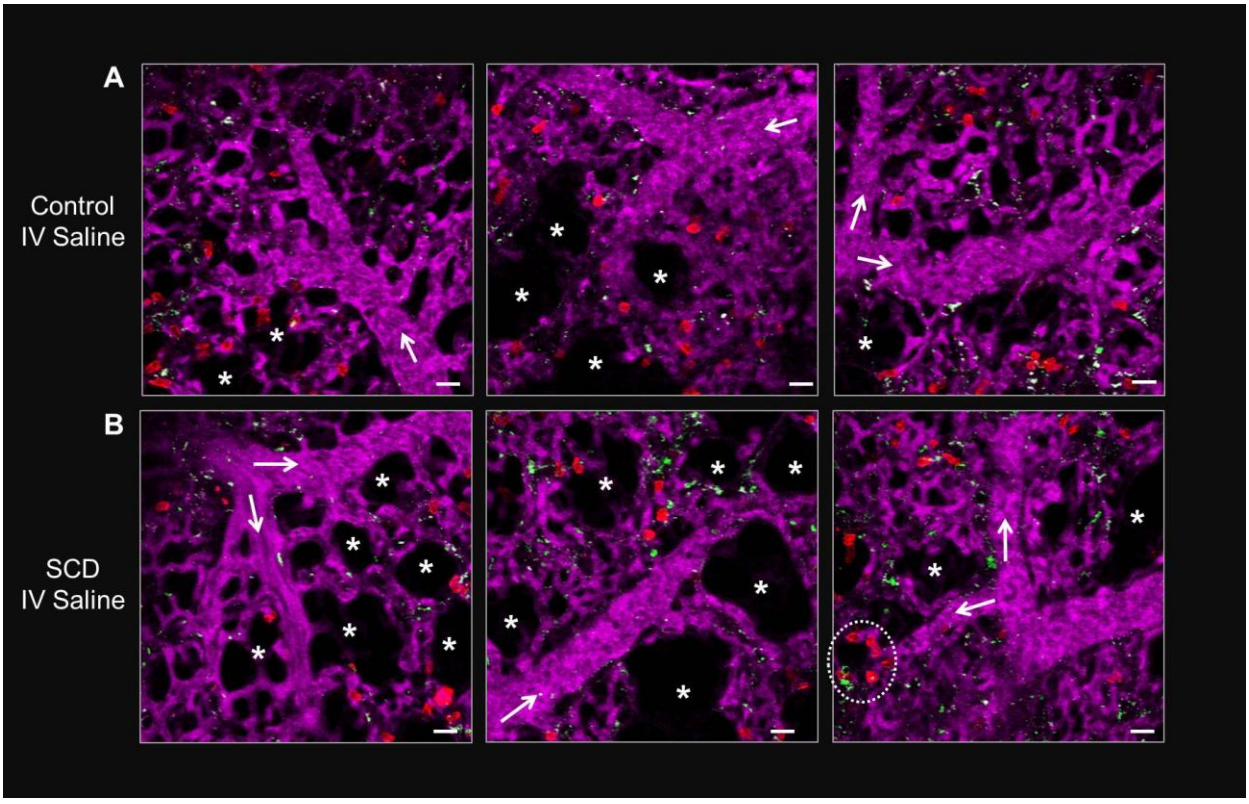

Figure S2. Pulmonary vaso-occlusion is minimal in the lungs of live BERK control and SCD mice following IV saline. Control and sickle cell disease (SCD) mice were injected intravenously (IV) with saline and pulmonary arterioles were imaged using quantitative fluorescence intravital lung microscopy (qFILM) to evaluate the presence of neutrophil-platelet aggregates blocking arteriolar bottle-necks. qFILM images are shown of 3 representative field of views (FOVs) from control and SCD mice administered with IV saline. (**A**) Pulmonary vaso-occlusions are minimal in control mice administered IV saline. (**B**) A majority of FOVs in SCD mice administered IV saline show no pulmonary vaso-occlusions (first and second FOVs). Occasional vaso-occlusions (white dotted circle) are seen blocking arteriolar branches. Shown is a neutrophil aggregate bound to a few platelets which is stuck in the arteriolar bottle-neck. Platelets (green) and neutrophils (red) were stained by IV administration of V450-CD49b mAb and AF546-Ly6G mAb, respectively. The pulmonary microcirculation including a feeding

arteriole and surrounding capillaries (purple) were visualized by IV administration of FITC-dextran. Pseudo-coloring was used for platelets and pulmonary vessels to enhance contrast. * denote the alveoli. White arrows mark the direction of blood flow within the feeding arterioles. The average diameters of the arterioles shown in **A**–**B** are: 36 ± 4 μm and 37 ± 5 μm, respectively. Scale bars are 20 μm. These images are selected from representative control and SCD mice administered with IV saline (total n = 3 control and n = 3 SCD mice; control = 23 FOVs; SCD = 29 FOVs).

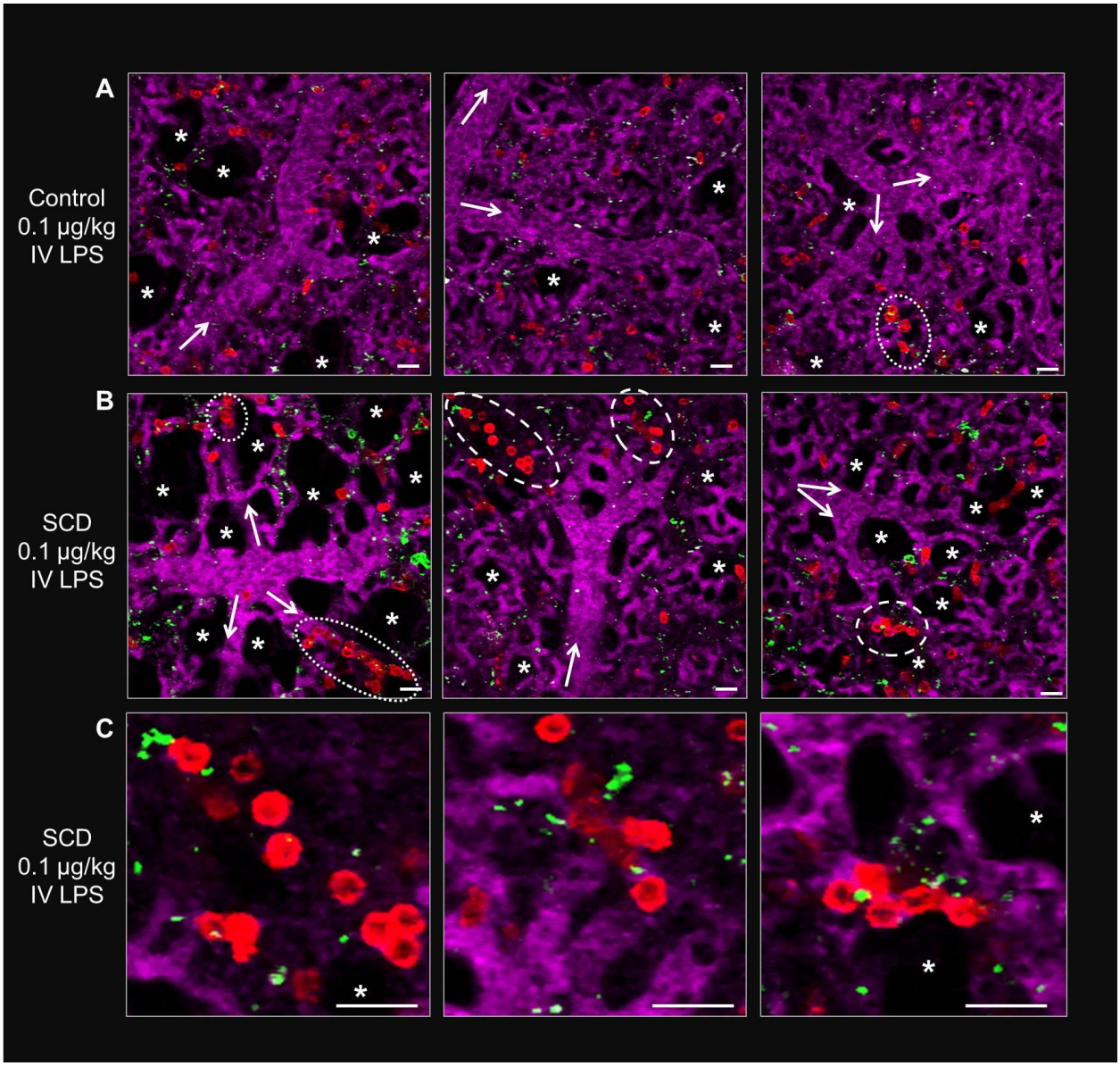

Figure S3. IV LPS (0.1 µg/kg) selectively triggers pulmonary vaso-occlusion in SCD but not control mice. Control and sickle cell disease (SCD) mice were injected intravenously (IV) with 0.1 µg/kg of lipopolysaccharide (LPS) and pulmonary arterioles were imaged using quantitative fluorescence intravital lung microscopy (qFILM) to evaluate the presence of neutrophil-platelet aggregates blocking the arteriolar bottle-necks. qFILM images are shown of 3 representative field of views (FOVs) from control and SCD mice administered with 0.1 µg/kg IV LPS. (**A**) 57% of FOVs in control mice administered 0.1 µg/kg IV LPS show no pulmonary vaso-occlusions

(first and second FOVs). (**A–B**) Characteristic pulmonary vaso-occlusions (white dotted circles), comprised of neutrophil aggregates bound to a few platelets, are shown blocking arteriolar branches. Control mice administered 0.1 μg/kg IV LPS (**A**) on average have smaller arteriolar vaso-occlusions compared to SCD mice challenged with 0.1 μg/kg IV LPS (**B**). (**C**) Magnified views of the arteriolar pulmonary vaso-occlusions are shown for the second and third FOVs of **B** (circles with longer dashes). Platelets (green) and neutrophils (red) were stained by IV administration of V450-CD49b mAb and AF546-Ly6G mAb, respectively. The pulmonary microcirculation including a feeding arteriole and surrounding capillaries (purple) were visualized by IV administration of FITC-dextran. Pseudo-coloring was used for platelets and pulmonary vessels to enhance contrast. * denote the alveoli. White arrows mark the direction of blood flow within the feeding arterioles. The average diameters of the arterioles shown in **A–B** are: 33 ± 5 μm and 32 ± 3 μm, respectively. Scale bars are 20 μm. These images are selected from representative control and SCD mice administered with 0.1 μg/kg IV LPS (total n = 5 control and n = 5 SCD mice; control = 54 FOVs; SCD = 48 FOVs). Images from Figure 1 are repeated here for convenience. Refer to Movies S3 and S4 for complete qFILM time series of the first two FOVs shown in **B**.

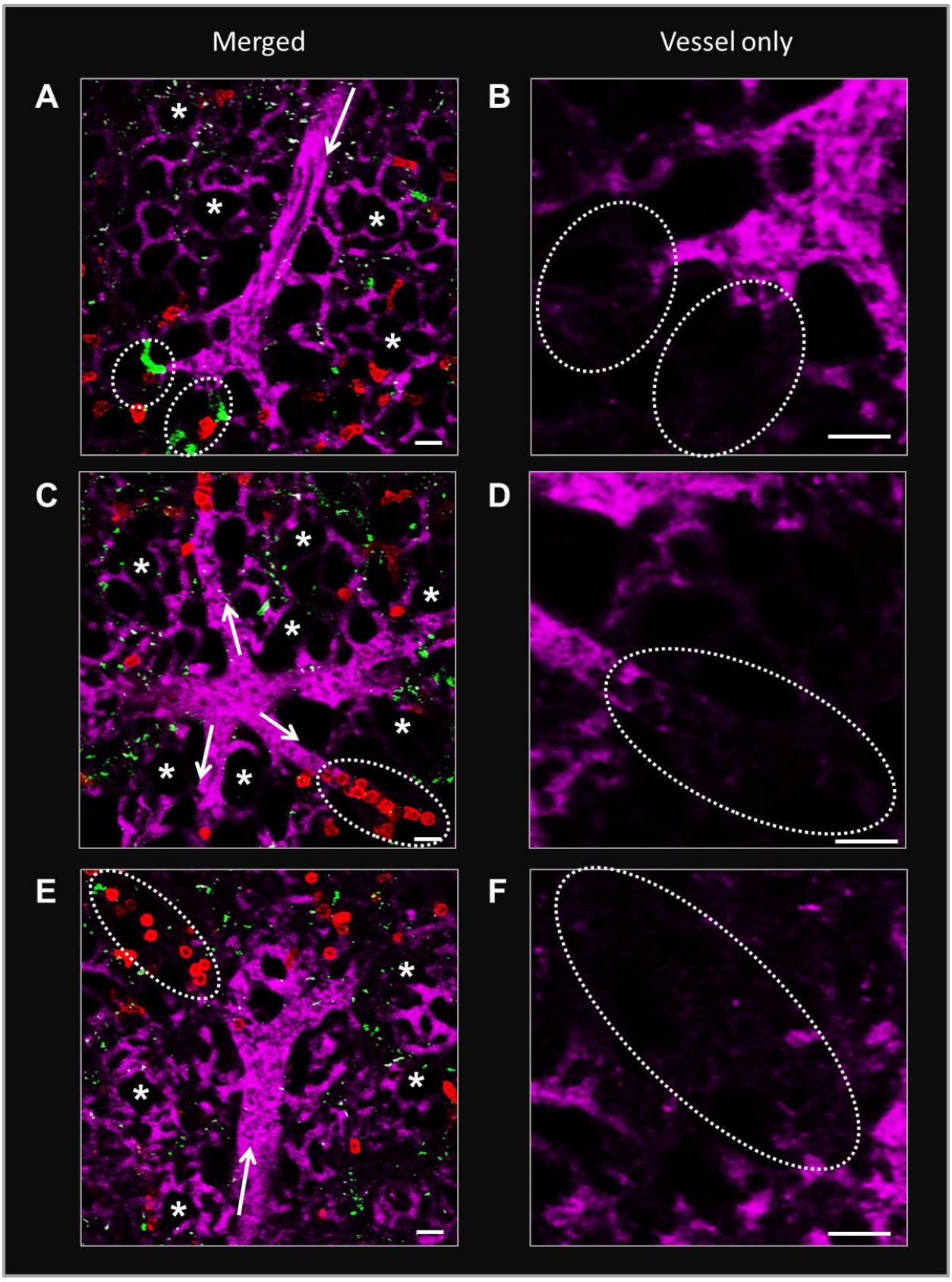
Merged
Vessel only
A
B
C
D
E
F

Figure S4. Neutrophil-platelet aggregates block the blood flow in arteriolar bottle-necks. Sickle cell disease (SCD) mice were injected intravenously (IV) with 0.1 µg/kg of lipopolysaccharide (LPS) and pulmonary arterioles were imaged using quantitative fluorescence intravital lung microscopy (qFILM) to determine whether neutrophil-platelet aggregates obstructed blood flow. qFILM images of 3 representative field of views (FOVs) in SCD mice administered 0.1 µg/kg IV LPS are shown. Neutrophil-platelet aggregates within the arteriolar bottle-necks (marked with dotted circles in merged images **A, C** and **E**) have a black background due to the lack of vessel dye (purple fluorescence absent in the magnified views **B, D** and **F** of regions marked with dotted circles in **A, C** and **E,** respectively), indicating an absence of blood flow downstream of the aggregates. Platelets (green) and neutrophils (red) were stained by IV administration of V450-CD49b mAb and AF546-Ly6G mAb, respectively. The pulmonary microcirculation including a feeding arteriole and surrounding capillaries (purple) were visualized by IV administration of FITC-dextran (shown purple). Pseudo-coloring was used for platelets and pulmonary vessels to enhance contrast. * denote the alveoli. White arrows mark the direction of blood flow within the feeding arterioles. The average diameter of the arterioles shown in **A, C** and **E** is 29 ± 5 µm respectively. Scale bars are 20 µm. These images are selected from 2 representative SCD mice administered with 0.1 µg/kg IV LPS (n=5 mice per group; SCD = 48 FOVs).

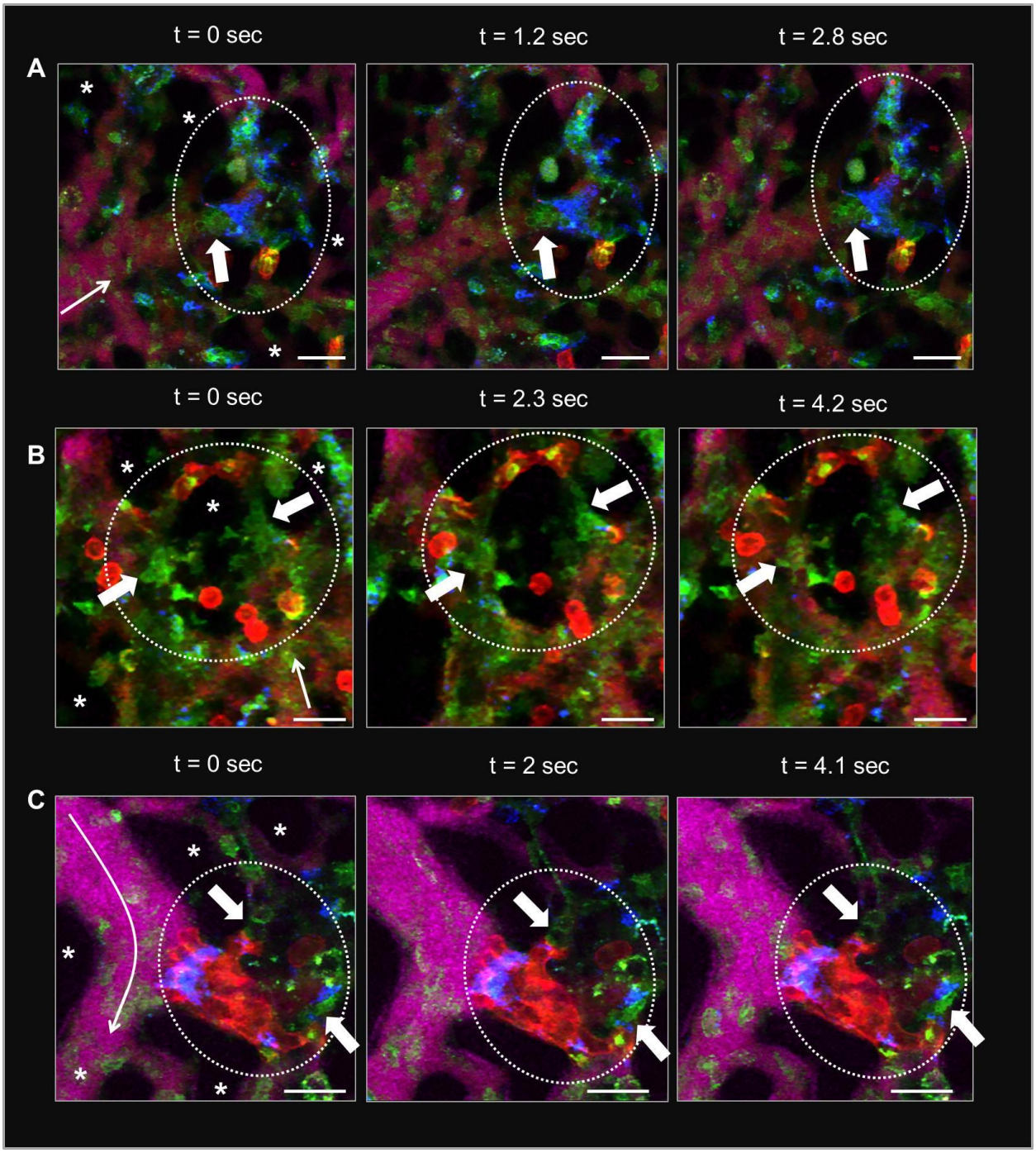

Figure S5. Erythrocyte transit is blocked by neutrophil-platelet aggregates in the arteriolar bottle-necks. Sickle cell disease (SCD) mice were injected intravenously (IV) with 0.1 µg/kg of lipopolysaccharide (LPS) and pulmonary arterioles were imaged using quantitative fluorescence intravital lung microscopy (qFILM) to determine whether neutrophil-platelet aggregates blocked

erythrocyte transit through the arteriole. qFILM images of 3 field of views (FOVs) at 3 different time points in SCD mice administered 0.1 µg/kg IV LPS are shown. (**A**-**B**) Stationary erythrocytes (shown in green, marked by thick white arrows) can be seen behind a platelet (**A**) or neutrophil (**B**) vaso-occlusion (platelets blue, neutrophils red). In Movie S5 (same FOV as shown in **B**), erythrocytes pulse back and forth behind the neutrophil aggregates, which indicates blockage of blood flow. (**C**) The erythrocytes downstream of the neutrophil-platelet aggregate (thick white arrows) are stationary while the ones upstream of the aggregate are bypassing the aggregate by transiting through the side branch of the arteriole (refer to Movie S6) suggesting that the neutrophil-platelet aggregate has blocked the blood flow in the arteriole. Dotted circles highlight cellular aggregates and regions of erythrocyte stasis. Platelets, neutrophils and erythrocytes were stained by IV administration of V450-CD49b mAb (blue), AF546-Ly6G mAb (red) and FITC-Ter119 mAb (green), respectively. The pulmonary microcirculation including a feeding arteriole and surrounding capillaries were visualized by IV administration of Evans blue (purple). * denote the alveoli. Thin white arrows mark the direction of blood flow within the feeding arterioles. The times displayed are relative to the selected video frames. The average diameter of the arterioles shown in **A**-**C** is 28 ± 3 µm. Scale bars are 20 µm. These images are selected from 1 representative SCD mouse administered with 0.1 µg/kg IV LPS (total n = 3 SCD mice; SCD = 62 FOVs). In Movies S5-S6, there is a slight rhythmic movement due to the ventilation of the mouse.

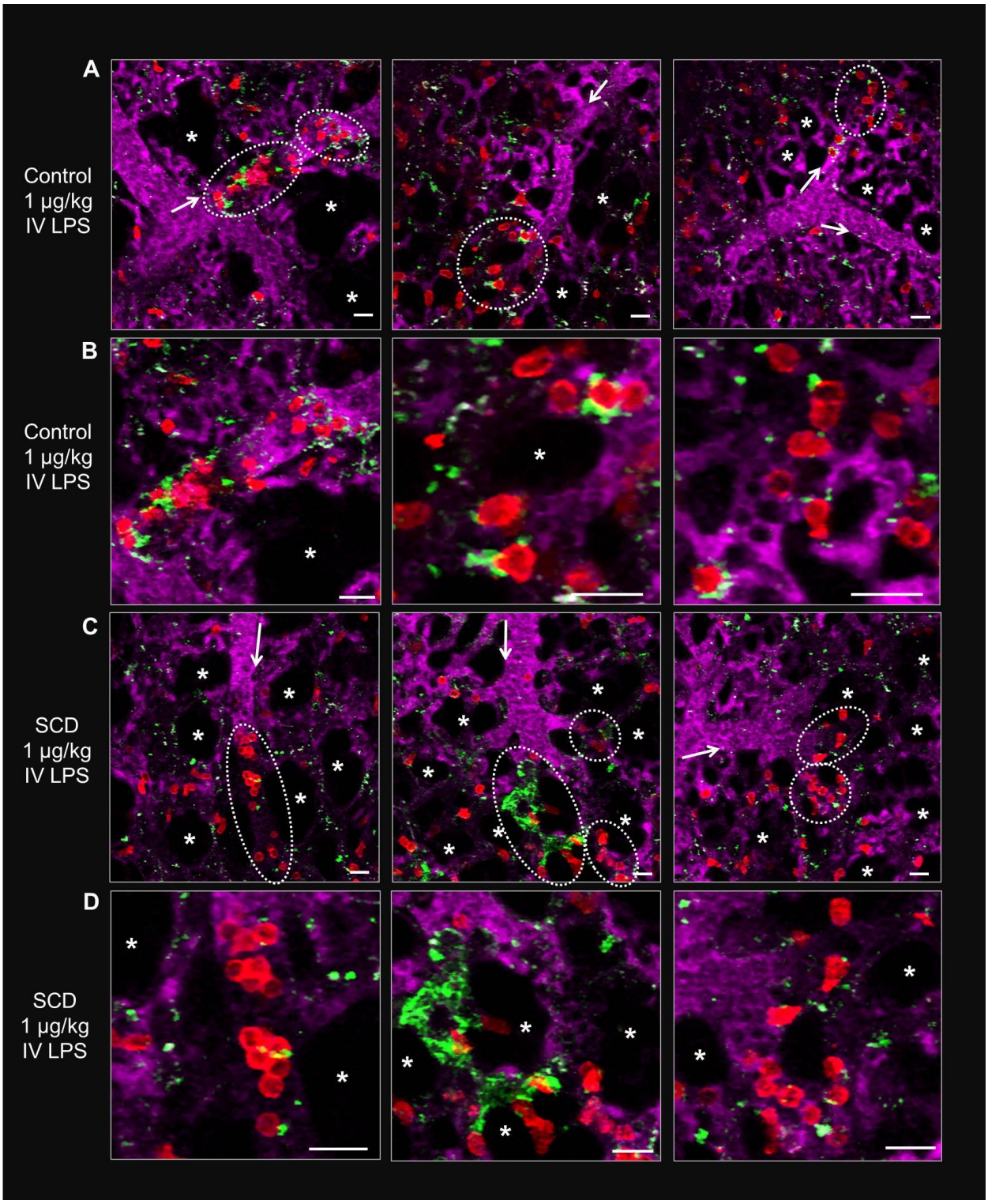
A
Control
1 µg/kg
IV LPS
B
Control
1 µg/kg
IV LPS
C
SCD
1 µg/kg
IV LPS
D
SCD
1 µg/kg
IV LPS

Figure S6. Ten folds higher dose of IV LPS (1 µg/kg) induces pulmonary vaso-occlusion in both control and SCD mice. Control and sickle cell disease (SCD) mice were injected intravenously (IV) with 1 µg/kg of lipopolysaccharide (LPS) and pulmonary arterioles were imaged using quantitative fluorescence intravital lung microscopy (qFILM) to evaluate the presence of neutrophil-platelet aggregates blocking arteriolar bottle-necks. qFILM images are shown of 3 representative field of views (FOVs) from control and SCD mice administered with 1 µg/kg IV LPS. Both control (**A-B**) and SCD (**C-D**) mice challenged with 1 µg/kg IV LPS exhibit pulmonary vaso-occlusions with increased numbers of neutrophil-platelet aggregates trapped in arteriolar bottle-necks. Characteristic vaso-occlusions blocking arteriolar branches are marked by dotted white circles (**A,C**) and the magnified views are shown below (**B,D**). Platelets (green) and neutrophils (red) were stained by IV administration of V450-CD49b mAb and AF546-Ly6G mAb, respectively. The pulmonary microcirculation including a feeding arteriole and surrounding capillaries (purple) were visualized by IV administration of FITC-dextran. Pseudo-coloring was used for platelets and pulmonary vessels to enhance contrast. * denote the alveoli. White arrows mark the direction of blood flow within the feeding arterioles. The average diameters of the arterioles shown in **A-B** and **C-D** are: 31 ± 4 µm and 31 ± 3 µm, respectively. Scale bars are 20 µm. These images are selected from 1 representative control and SCD mouse administered with 1 µg/kg IV LPS (total n = 3 control and n = 3 SCD mice; control = 25 FOVs; SCD = 31 FOVs).

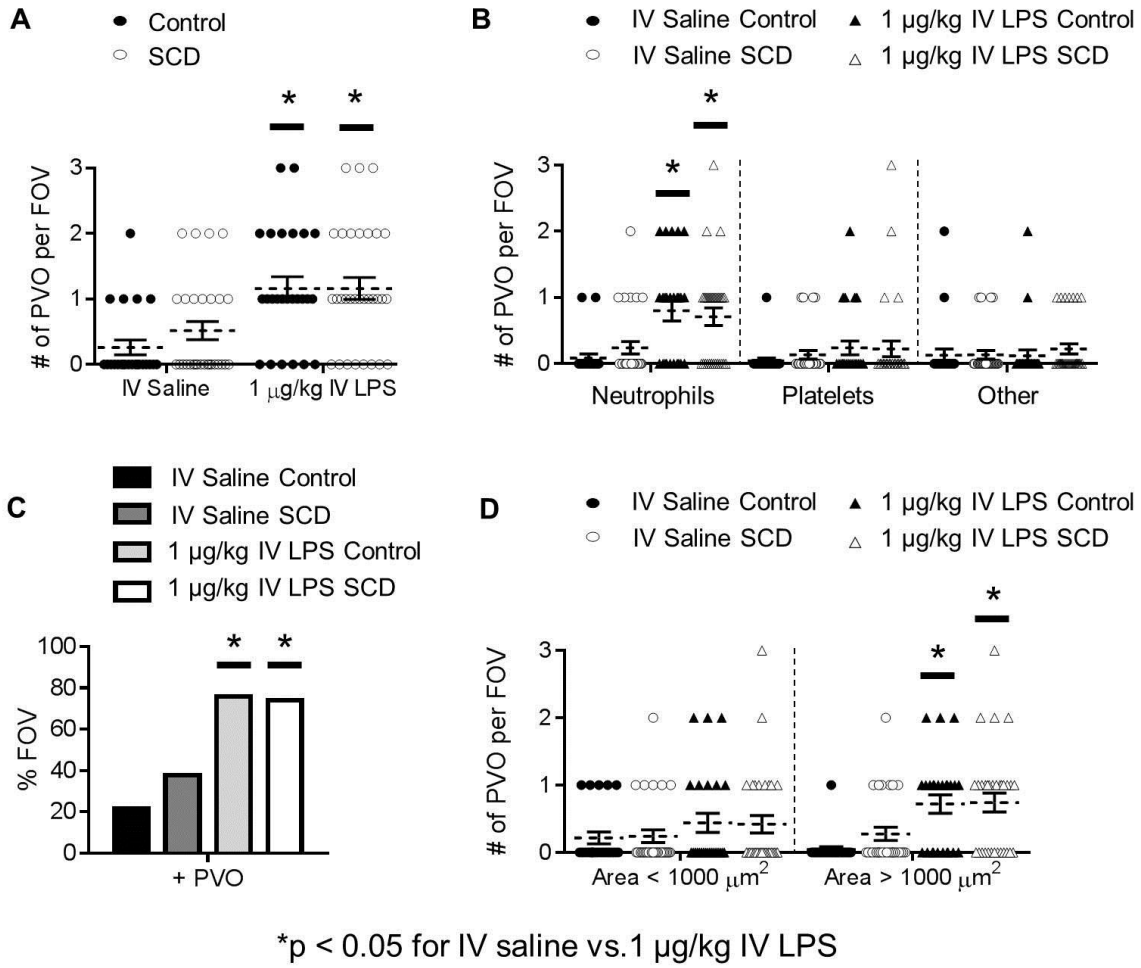

Figure S7. Ten folds higher dose of IV LPS (1 μg/kg) promotes pulmonary vaso-occlusion in both control and SCD mice. Control and sickle cell disease (SCD) mice were injected intravenously (IV) with saline (n=3 mice per group; control = 23 field of views, FOVs; SCD = 29 FOVs) or 1 μg/kg of lipopolysaccharide (LPS) (n=3 mice per group; control = 25 FOVs; SCD = 31 FOVs). Pulmonary arterioles were imaged 2 to 2.5 h post IV saline or 1 μg/kg IV LPS using quantitative fluorescence intravital lung microscopy (qFILM). Pulmonary vaso-occlusions in arterioles were characterized and quantified using the nomenclature described in the Supplementary Methods section. Data from control and SCD mice + IV saline is repeated from Figure 1 for comparison. (**A**) Number of pulmonary vaso-occlusions per FOV for control (black

circles) and SCD mice (white circles) administered with either IV saline or IV LPS. Each FOV was 67,600 μm^2 in size. (**B**) Number of pulmonary vaso-occlusions per FOV classified by cellular composition: neutrophil vaso-occlusion (primarily neutrophils with few platelets), platelet vaso-occlusion (primarily platelets with few neutrophils) and other vaso-occlusion (primarily other cell types with few neutrophils and/or platelets). (**C**) Percent FOVs with pulmonary vaso-occlusions. (**D**) Number of pulmonary vaso-occlusions per FOV classified as having an area of $< 1000\ \mu m^2$ or $> 1000\ \mu m^2$. Refer to Supplementary Methods for details on measurement of vaso-occlusion area. The average number of pulmonary vaso-occlusions per FOV, the area of pulmonary vaso-occlusions, and cellular composition of pulmonary vaso-occlusions were compared using *t*-tests with Bonferroni correction. The percent FOVs with pulmonary vaso-occlusions were compared between different groups using fourfold table analyses with Bonferroni χ^2-statistics. Each data point represents a single FOV and observations were made over multiple FOVs per experiment. Data represents mean ± SEM. $^*p < 0.05$ for IV saline vs. 1 μg/kg IV LPS.

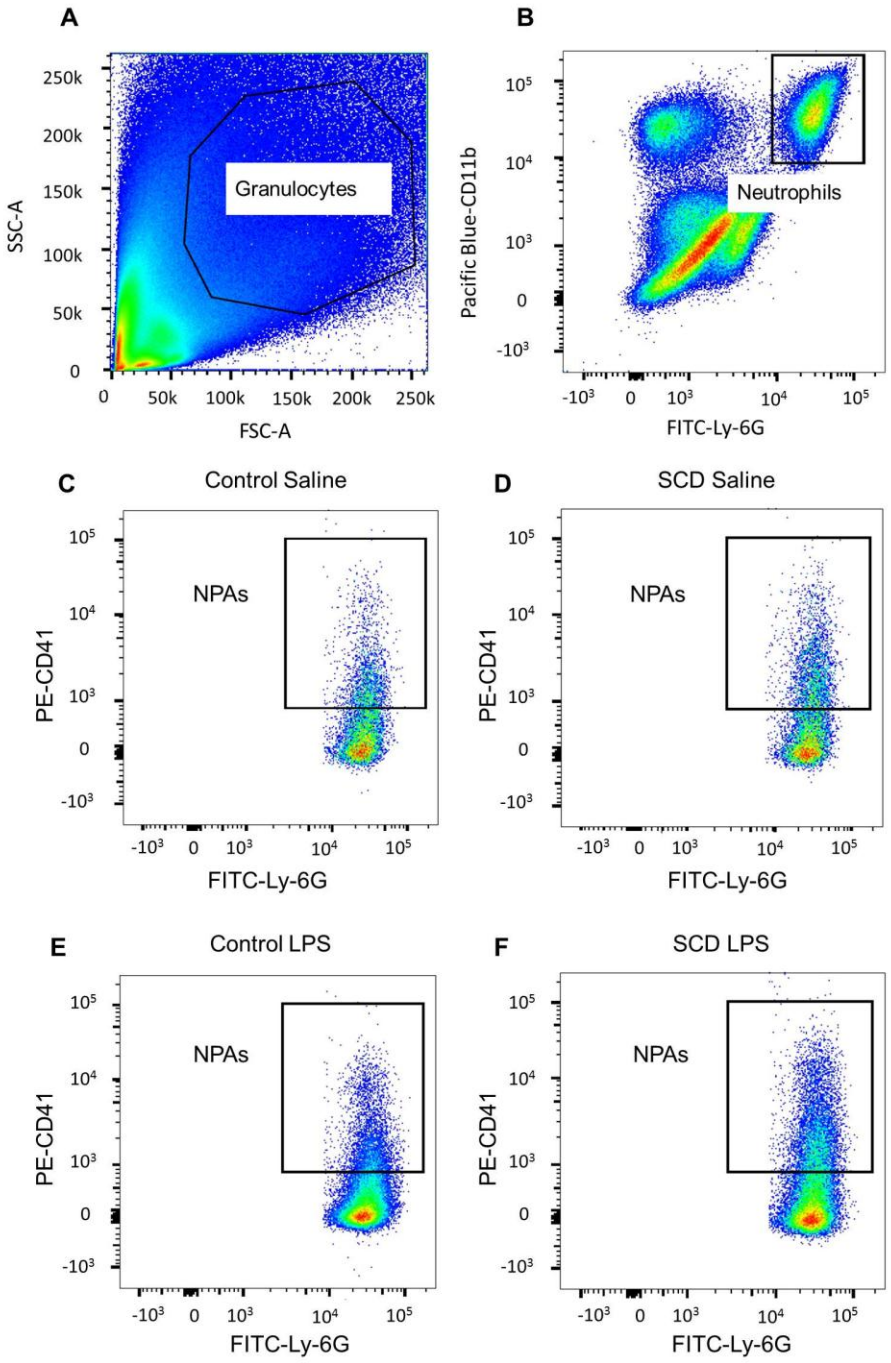

Figure S8. SCD mice have more neutrophil-platelet aggregates in the lung than control mice. Flow cytometry was used to compare the presence of neutrophil-platelet aggregates (NPAs) in digested whole lung cell suspensions at 2 to 2.5 hours following either intravenous (IV) saline (n = 5 mice per group) or 0.1 μg/kg IV lipopolysaccharide (LPS) (n = 4 mice per

group) administration. (**A**-**F**) Gating strategy for flow cytometry analysis of neutrophil-platelet aggregates. (**A**) A gate was drawn around the granulocyte population (SSC^{hi}/FSC^{hi}) on the side scatter vs. forward scatter plot and 100,000 to 150,000 events were recorded within the gate for each sample. (**B**) Neutrophils were defined as $FSC^{hi}/SSC^{hi}/Ly\text{-}6G^{+}/CD11b^{+}$. Thus, double positive cells for Pacific Blue-CD11b and FITC-Ly-6G were gated as the neutrophil population. (**C-F**) Neutrophil-platelet aggregates were defined as $Ly\text{-}6G^{+}/CD11b^{+}/CD41^{+}$. On the plot of PE-CD41 vs. FITC-Ly-6G, only the double positive cells were selected as neutrophil-platelet aggregates (inside square gates in **C**-**F**). Representative flow cytometry plots showing neutrophil-platelet aggregates in the whole lung digest are shown. (**C**) Control mouse challenged with IV saline. (**D**) SCD mouse challenged with IV saline. (**E**) Control mouse challenged with 0.1 μg/kg IV LPS. (**F**) SCD mouse challenged with 0.1 μg/kg IV LPS. The gating cut-offs for positive fluorescence signals in **B**-**F** were determined using the appropriate isotype control antibodies (refer to Supplementary Methods for details).

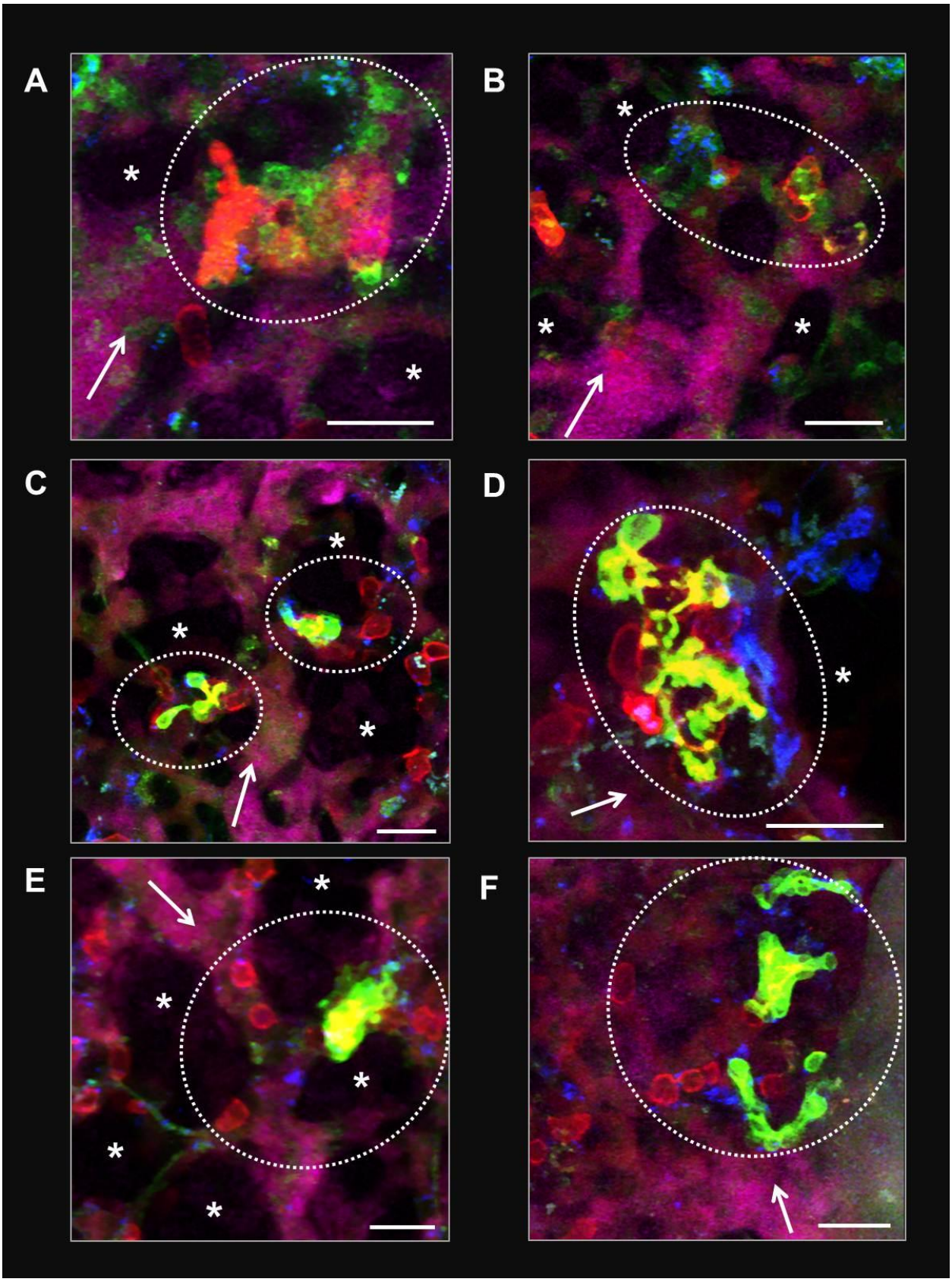
A
B
C
D
E
F

Figure S9. Erythrocytes are also present within neutrophil-platelet aggregates in arteriolar bottle-necks. Sickle cell disease (SCD) mice were injected intravenously (IV) with 0.1 µg/kg of lipopolysaccharide (LPS) and pulmonary arterioles were imaged using quantitative fluorescence intravital lung microscopy (qFILM) to determine whether erythrocytes were included within neutrophil-platelet aggregates. qFILM images of 6 different field of views (FOVs) in SCD mice administered 0.1 µg/kg IV LPS are shown. (**A-F**) Erythrocytes (green) are incorporated within neutrophil-platelet aggregates in arteriolar bottle-necks (neutrophils-red, platelets-blue) and remain stationary throughout the time series. Dotted circles highlight aggregates containing platelets, neutrophils and erythrocytes. In Movie S8 (FOV shown in **A**), erythrocytes are shown both inside the large neutrophil-platelet aggregate as well as stationary behind the aggregate. Movie S9 (FOV shown in **D**) shows erythrocytes present throughout the large neutrophil-platelet aggregate and a circulating neutrophil joining the neutrophil-platelet-erythrocyte aggregate at the end of the time series. In Movie S10 (FOV shown in **E**), the neutrophil-platelet-erythrocyte aggregate has blocked the blood flow resulting in back and forth pulsation of erythrocytes and a neutrophil that are behind the vaso-occlusion. Platelets, neutrophils and erythrocytes were stained by IV administration of V450-CD49b mAb (blue), AF546-Ly6G mAb (red) and FITC-Ter119 mAb (green), respectively. The pulmonary microcirculation including a feeding arteriole and surrounding capillaries were visualized by IV administration of Evans blue (purple). * denote the alveoli. White arrows mark the direction of blood flow within the feeding arterioles. The average diameter of the arterioles shown in **A-F** is 24 ± 5 µm. Scale bars are 20 µm. These images are selected from 2 representative SCD mice administered with 0.1 µg/kg IV LPS (total n = 3 SCD mice; SCD = 62 FOVs). In Movies S8-S10, there is a slight rhythmic movement due to the ventilation of the mouse.

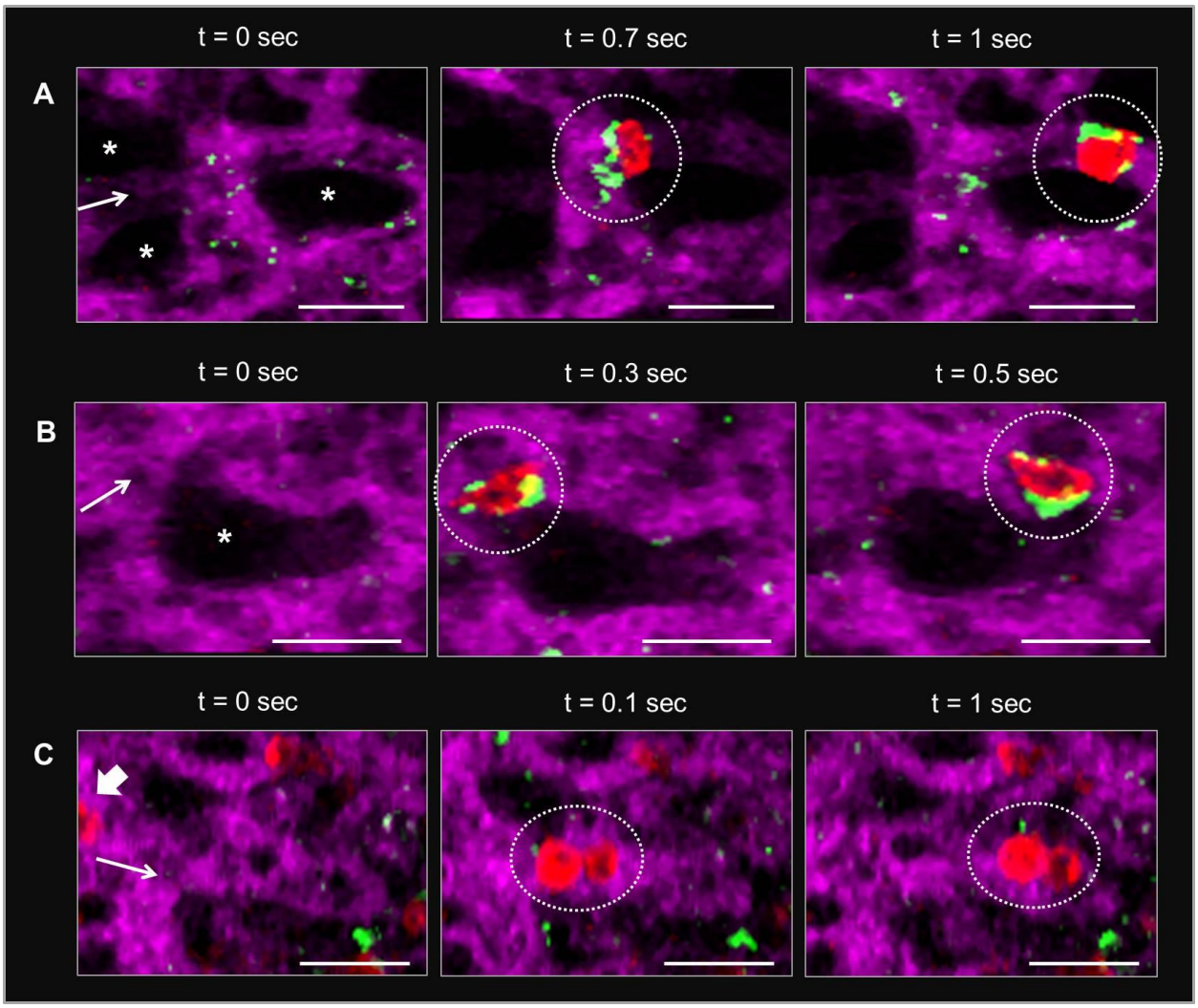

Figure S10. Circulating micro-embolic neutrophil-platelet aggregates contribute to pulmonary vaso-occlusion. Sickle cell disease (SCD) mice were injected intravenously (IV) with 0.1 µg/kg of lipopolysaccharide (LPS) and pulmonary arterioles were imaged using quantitative fluorescence intravital lung microscopy (qFILM) to determine whether pulmonary vaso-occlusion involves occlusion of arteriolar bottle-necks by embolic neutrophil-platelet aggregates. qFILM images of 3 field of views (FOVs) at 3 different time points in SCD mice administered 0.1 µg/kg IV LPS are shown. (**A**) A circulating neutrophil-platelet aggregate is shown transiting through the pulmonary arteriole. The arteriolar bottle-neck is free of aggregates

at t = 0 s. A preformed neutrophil-platelet aggregate appears in the arteriole at t = 0.7 s and transits through the bottle-neck by t = 1 s. This representative example demonstrates that preformed neutrophil-platelet aggregates are present in the blood circulation of SCD mice administered 0.1 µg/kg IV LPS. Refer to Movie S12 (FOV shown in **A**) to see the neutrophil covered in platelets transiting through the pulmonary arteriole. (**B**) A circulating neutrophil-platelet embolic aggregate consisting of a neutrophil coated with platelets arrives in the pulmonary arteriole at t = 0.3 s and stops in the arteriolar bottle-neck by t = 0.5 s. Refer to Movie S13 (FOV shown in **B**) for the complete time series. (**C**) A small micro-embolic neutrophil-platelet aggregate stops within the arteriolar bottle-neck. At t = 0 s, the aggregate begins to appear in the FOV (thick white arrow). At t = 0.1 s, the aggregate which is comprised of two neutrophils bound to a few platelets (white dotted circle) begins to travel down the arteriole. The embolic aggregate stops in the arteriolar bottle-neck by t = 1 s. The times displayed are relative to the selected frames. Platelets (green) and neutrophils (red) were stained by IV administration of V450-CD49b mAb and AF546-Ly6G mAb, respectively. The pulmonary microcirculation including a feeding arteriole and surrounding capillaries (purple) were visualized by IV administration of FITC-dextran. Pseudo-coloring was used for platelets and pulmonary vessels to enhance contrast. * denote the alveoli. White arrows mark the direction of blood flow within the feeding arterioles. The average diameter of the arterioles shown in **A-C** is 32 ± 6 µm. Scale bars are 20 µm. These images are selected from 2 representative SCD mice administered with 0.1 µg/kg IV LPS (total n = 7 SCD mice; SCD = 84 FOVs). In Movies S12-S13, there is a slight rhythmic movement due to the ventilation of the mouse.

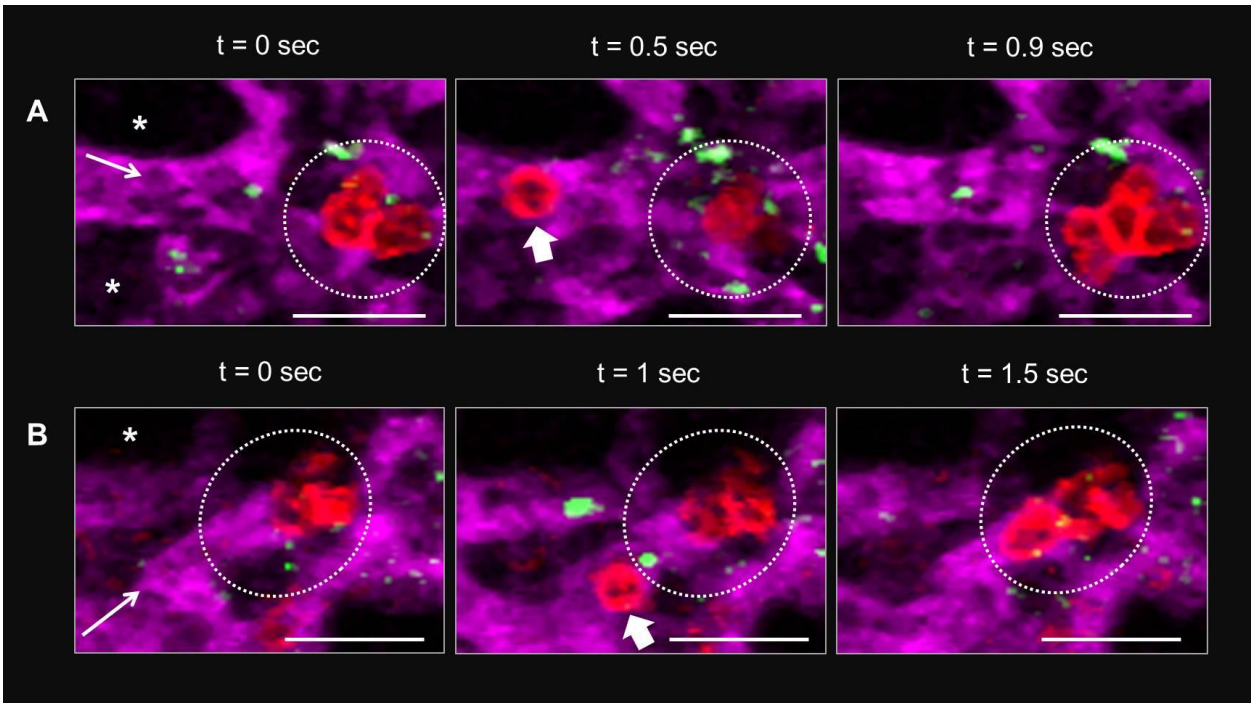

Figure S11. Neutrophil-platelet aggregates formed by in situ nucleation occlude the arteriolar bottle-necks. Sickle cell disease (SCD) mice were injected intravenously (IV) with 0.1 µg/kg of lipopolysaccharide (LPS) and pulmonary arterioles were imaged using quantitative fluorescence intravital lung microscopy (qFILM) to determine whether neutrophil-platelet aggregates can also form in the arteriolar bottle-neck by in situ nucleation of individual neutrophils and platelets. qFILM images of 2 field of views (FOVs) at 3 different time points in SCD mice administered 0.1 µg/kg IV LPS are shown. (**A**-**B**) Single circulating neutrophils (thick white arrows) nucleate on pre-existing neutrophil-platelet aggregates (dotted white circles) within the arteriolar bottle-necks to promote pulmonary vaso-occlusions. Movies S15 and S16 (FOVs shown in **A** and **B**, respectively), both highlight single circulating neutrophils adhering to pre-existing small aggregates of 3 neutrophils attached to a few platelets within the arteriolar bottle-necks. In the time series, there is a slight rhythmic movement due to the ventilation of the mouse. The times displayed are relative to the selected frames. Platelets (green) and neutrophils

(red) were stained by IV administration of V450-CD49b mAb and AF546-Ly6G mAb, respectively. The pulmonary microcirculation including a feeding arteriole and surrounding capillaries (purple) were visualized by IV administration of FITC-dextran. Pseudo-coloring was used for platelets and pulmonary vessels to enhance contrast. * denote the alveoli. White arrows mark the direction of blood flow within the feeding arterioles. The diameter of the arterioles shown in **A** and **B** is 30 μm and 29 μm, respectively. Scale bars are 20 μm. These images are selected from 2 representative SCD mice administered with 0.1 μg/kg IV LPS (total n = 7 SCD mice; SCD = 84 FOVs).

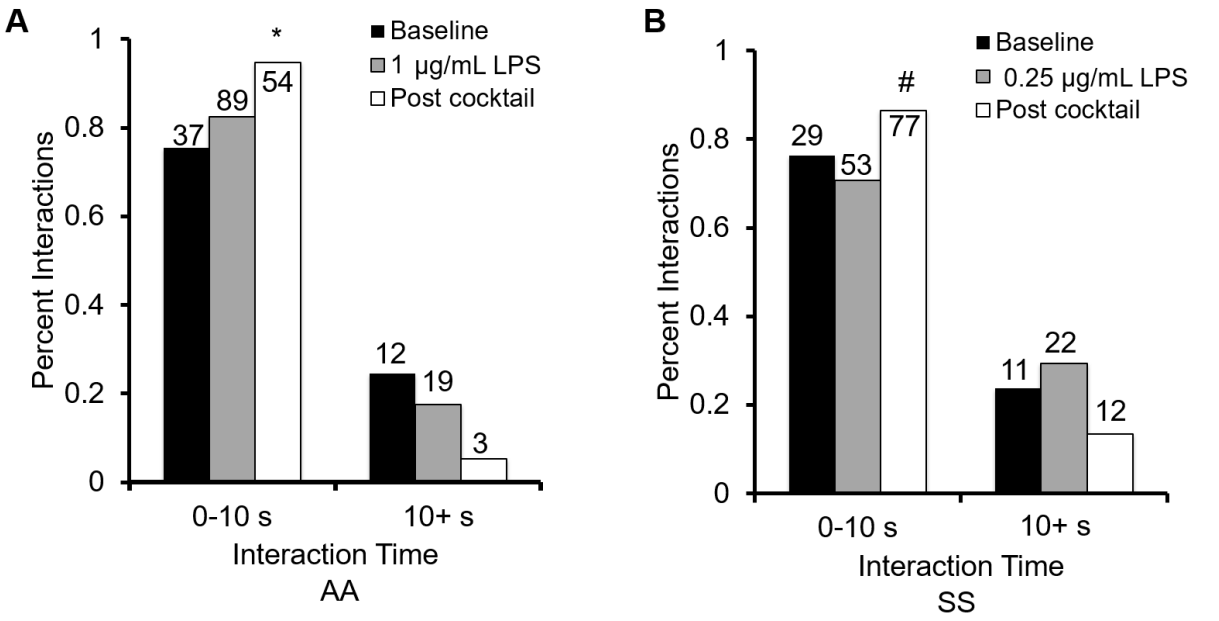

Figure S12. Effect of P-selectin/CD11b Abs on lifetime of neutrophil-platelet interactions in LPS treated human blood. Percent of total platelet-neutrophil interaction events in (**A**) control (AA) and (**B**) SCD (SS) human blood with a lifetime of either 0-10 s or greater than 10 s. Control or SCD human whole blood with or without LPS (0.25 or 1 μg/ml) and with or without addition of function blocking cocktail (combination of anti-Mac-1 and anti-P-selectin mAbs) was perfused through micro-channels presenting P-selectin, ICAM-1 and IL-8, and platelet interactions with arrested neutrophils were assessed over a 2 min period using qMFM. Wall shear stress: 6 dynes cm^{-2}. FOV (field of view) ~ 14,520 μm^2. * $p<0.05$ when compared to baseline. # $p<0.05$ when compared to LPS. Based on >45 randomly selected events per condition from 7 experiments using 3 control and 4 SCD patients. Fourfold table analysis with Bonferroni χ^2 statistics was used to compare percent interaction times. Numbers on graph represent the number of data points included in each treatment group.

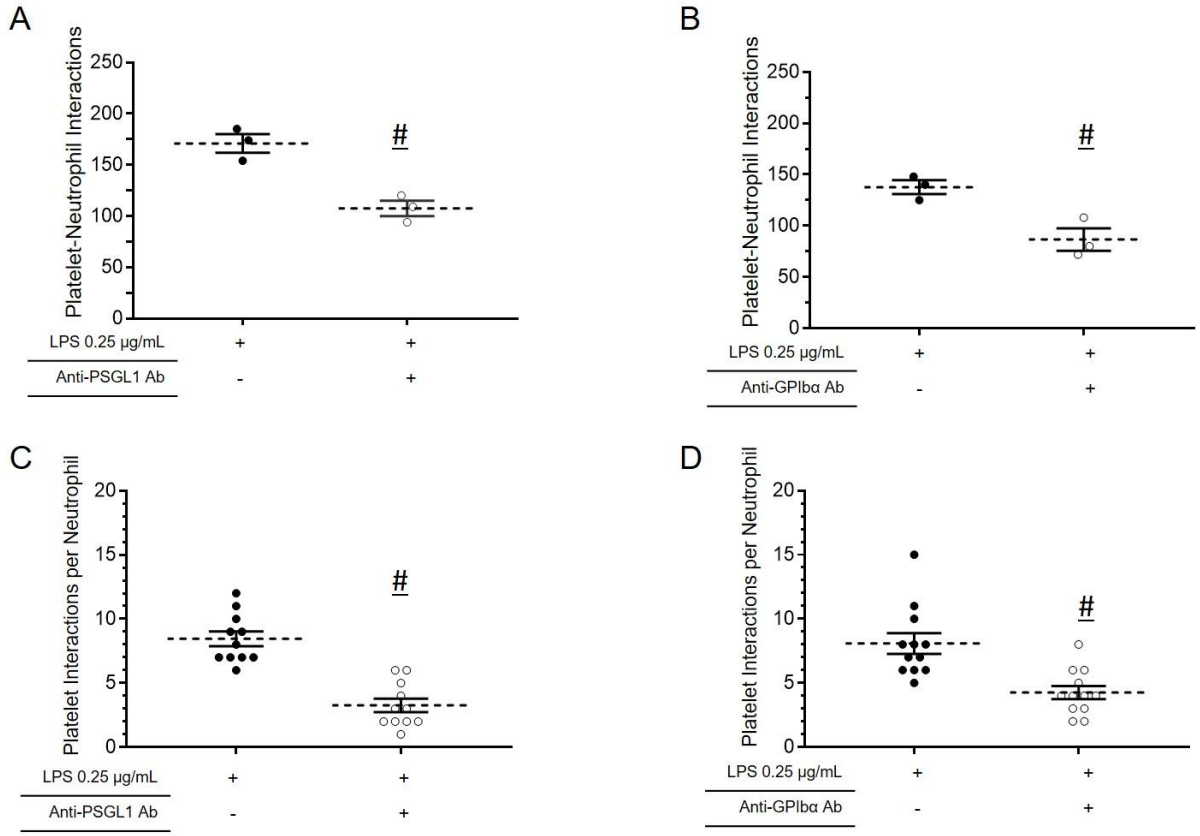

Figure S13. PSGL-1 or GPIbα blockade inhibits neutrophil-platelet interactions in LPS treated SCD human blood. Steady state SCD (SS) human whole blood was treated with 0.25 µg/ml of LPS and perfused through microfluidic channels with or without addition of blocking mAbs against either PSGL-1 (**A**,**C**) or GPIbα (**B**,**D**). Total platelet-neutrophil interactions and platelet interactions per neutrophil were observed over multiple FOVs. PSGL-1 and GPIbα mAbs significantly reduced the total platelet-neutrophil interactions and platelet interactions per neutrophil in SCD human blood treated with LPS. Interactions were counted as described in Supplementary Methods. Data was generated from 2 experiments done with two SS patients. Data represents mean ± SEM. Each data point represents a single FOV and observations were

made over multiple FOVs per experiment. Wall shear stress 6 dynes cm^{-2}. FOV (field of view) ~ 14,520 μm^2. # $p<0.05$ when compared to LPS treatment.

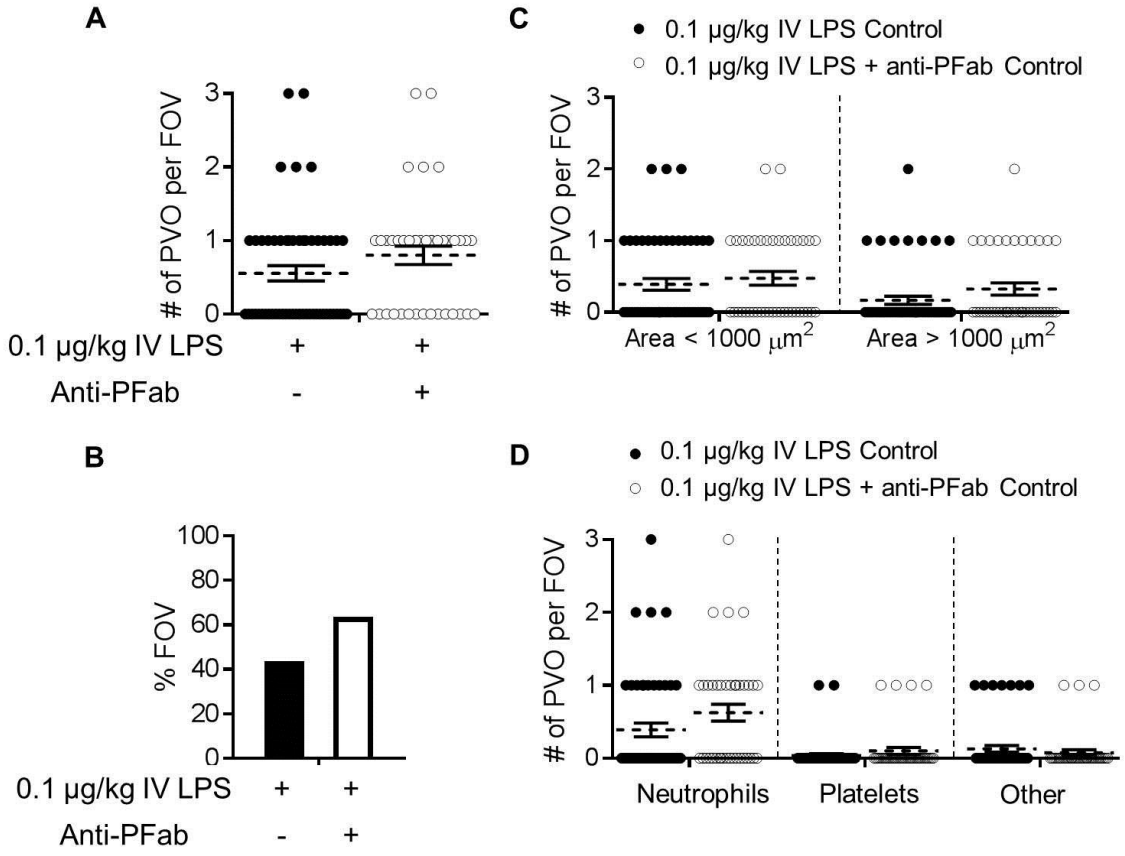

Figure S14. P-selectin blockade did not affect the LPS-induced pulmonary vaso-occlusions in control mice. Control mice were injected intravenously (IV) with 0.1 µg/kg of lipopolysaccharide (LPS) only (n=5 mice per group; control = 54 field of views, FOVs) or 0.1 µg/kg IV LPS + anti-P-selectin mAb Fab fragments (n=3 mice per group; control = 40 FOVs). Pulmonary arterioles were imaged 2 to 2.5 h post IV LPS or post IV LPS + anti-P-selectin mAb Fab fragments using quantitative fluorescence intravital lung microscopy (qFILM). Pulmonary vaso-occlusions in arterioles were characterized and quantified using the nomenclature described in the Supplementary Methods section. Data from control mice + 0.1 µg/kg IV LPS is repeated from Figure 1 for comparison. (**A**) Number of pulmonary vaso-occlusions per FOV in control mice administered with either IV LPS (black circles) or IV LPS + anti-P-selectin mAb Fab

fragments (white circles). Each FOV was 67,600 μm^2 in size. (**B**) Percent FOVs with pulmonary vaso-occlusions. (**C**) Number of pulmonary vaso-occlusions per FOV classified as having an area of < 1000 μm^2 or > 1000 μm^2. Refer to Supplementary Methods for details on measurement of vaso-occlusion area. (**D**) Number of pulmonary vaso-occlusions per FOV classified by cellular composition: neutrophil vaso-occlusion (primarily neutrophils with few platelets), platelet vaso-occlusion (primarily platelets with few neutrophils) and other vaso-occlusion (primarily other cell types with few neutrophils and/or platelets). The average number of pulmonary vaso-occlusions per FOV, the area of pulmonary vaso-occlusions, and cellular composition of pulmonary vaso-occlusions were compared using unpaired *t*-tests. The percent of FOVs with pulmonary vaso-occlusions were compared between different groups using fourfold table analyses with Bonferroni χ^2-statistics. Each data point represents a single FOV and observations were made over multiple FOVs per experiment. Data represents mean ± SEM. No comparisons were statistically significant.

LEGENDS FOR SUPPLEMENTARY MOVIES

Movie S1. Neutrophils (red) and platelets (green) trafficking through the pulmonary microcirculation (purple) in a control mouse after IV saline administration. A freely circulating neutrophil is seen trafficking up the arteriole into the capillaries. Pulmonary vaso-occlusion is absent. 2/3x original acquisition rate.

Movie S2. Neutrophils (red) and platelets (green) trafficking through the pulmonary microcirculation (purple) in a SCD mouse after IV saline administration. A freely circulating neutrophil is seen trafficking up the arteriole into the capillaries. Pulmonary vaso-occlusion is absent. 2/3x original acquisition rate.

Movie S3. Two pulmonary vaso-occlusions blocking arteriolar bottle-necks in a SCD mouse administered 0.1 µg/kg IV LPS. A large and a small aggregate of neutrophils (red) and a few platelets (green) are marked by white circles. Pulmonary microcirculation (purple). 2/3x original acquisition rate.

Movie S4. Two pulmonary vaso-occlusions blocking arteriolar bottle-necks in a SCD mouse administered 0.1 µg/kg IV LPS. Two large aggregates of neutrophils (red) and a few platelets (green) are marked by white circles. Pulmonary microcirculation (purple). 2/3x original acquisition rate.

Movie S5. Erythrocyte stasis behind a neutrophil vaso-occlusion in a SCD mouse administered 0.1 µg/kg IV LPS. Neutrophils (red) bound to a few platelets (blue) are occluding the arteriolar bottleneck. Erythrocytes (green) are pulsating back and forth behind the vaso-occlusion. White arrow-direction of blood flow. Pulmonary microcirculation (purple). 2/3x original acquisition rate.

Movie S6. Neutrophils (red) bound to platelets (blue) are occluding the arteriolar bottleneck in a SCD mouse administered 0.1 µg/kg IV LPS. Erythrocytes (green) are stationary downstream of the vaso-occlusion but erythrocytes upstream of the vaso-occlusion are colliding with the aggregate and then bypassing through the side branch of the arteriole. White arrow-direction of blood flow. Pulmonary microcirculation (purple). 1/3x original acquisition rate.

Movie S7. Pulmonary vaso-occlusions (white circles) blocking all 4 arteriolar bottle-necks in a SCD mouse administered 0.1 µg/kg IV LPS. Neutrophil vaso-occlusions (red arrows). Platelet vaso-occlusions (green arrows). White arrow-direction of blood flow. Pulmonary microcirculation (purple). 2/3x original acquisition rate.

Movie S8. Erythrocytes present within a neutrophil-platelet aggregate in a SCD mouse administered 0.1 µg/kg IV LPS. A large aggregate of neutrophils (red), a few platelets (blue), and erythrocytes (green) is occluding the arteriolar bottleneck. Erythrocytes (green) are pulsating behind the aggregate indicating blockage of blood flow. White arrow-direction of blood flow. Pulmonary microcirculation (purple). 1/3x original acquisition rate.

Movie S9. Erythrocytes present within a neutrophil-platelet aggregate in a SCD mouse administered 0.1 µg/kg IV LPS. A large aggregate of neutrophils (red), platelets (blue) and erythrocytes (green) is occluding the arteriolar bottleneck. A circulating neutrophil adds to the vaso-occlusion at the end of the video. White arrow-direction of blood flow. Pulmonary microcirculation (purple). 1/3x original acquisition rate.

Movie S10. Erythrocytes present within a neutrophil-platelet aggregate in a SCD mouse administered 0.1 µg/kg IV LPS. A large aggregate of neutrophils (red), a few platelets (blue) and erythrocytes (green) is occluding the arteriolar bottleneck. Erythrocytes and a neutrophil are seen pulsating upstream of the aggregate. White arrow-direction of blood flow. Pulmonary microcirculation (purple). 2/3x original acquisition rate.

Movie S11. Embolic neutrophil-platelet aggregate occluding an arteriole in a SCD mouse administered 0.1 µg/kg IV LPS. A large aggregate of several neutrophils (red) with a few platelets (green) travels down the feeding arteriole and occludes the arteriolar bottle-neck. Pulmonary microcirculation (purple). 2/3x original acquisition rate.

Movie S12. Circulating embolic neutrophil-platelet aggregate transiting through an arteriole in a SCD mouse administered 0.1 µg/kg IV LPS. A neutrophil (red) coated with platelets (green) travels down the feeding arteriole and disappears downstream. White arrow-direction of blood flow. Pulmonary microcirculation (purple). 1/3x original acquisition rate.

Movie S13. Circulating embolic neutrophil-platelet aggregate stops in the arteriolar bottle-neck in a SCD mouse administered 0.1 µg/kg IV LPS. Neutrophil (red) coated with platelets (green). White arrow-direction of blood flow. Pulmonary microcirculation (purple). 1/3x original acquisition rate.

Movie S14. In situ nucleation of a neutrophil-platelet aggregate in the pulmonary arteriolar bottle-neck in a SCD mouse administered 0.1 µg/kg IV LPS. An aggregate (white circle) of three neutrophils (red) attached to a few platelets (green) slowly grows over time to an aggregate of five neutrophils which completely blocks an arteriolar branch. Pulmonary microcirculation (purple). 2/3x original acquisition rate.

Movie S15. In situ nucleation of a neutrophil-platelet aggregate in the pulmonary arteriolar bottle-neck in a SCD mouse administered 0.1 µg/kg IV LPS. A small aggregate of neutrophils (red) bound to a few platelets (green) grows over time with the addition of a circulating neutrophil. White arrow-direction of blood flow. Pulmonary microcirculation (purple). 1/3x original acquisition rate.

Movie S16. In situ nucleation of a neutrophil-platelet aggregate in the pulmonary arteriolar bottle-neck in a SCD mouse administered 0.1 µg/kg IV LPS. A small aggregate of neutrophils (red) bound to a few platelets (green) grows over time with the addition of a circulating neutrophil. White arrow-direction of blood flow. Pulmonary microcirculation (purple). 1/3x original acquisition rate.

Movie S17. Freely flowing platelets interacting with arrested neutrophils in control human blood perfused through microfluidic micro-channels presenting P-selectin, ICAM-1 and IL-8. qMFM acquisition (10 frames s^{-1}). Neutrophils (purple). Platelets (green). Wall shear stress 6 dyn cm^{-2}.

Movie S18. Freely flowing platelets interacting with arrested neutrophils in SCD human blood perfused through microfluidic micro-channels presenting P-selectin, ICAM-1 and IL-8. qMFM acquisition (10 frames s^{-1}). Neutrophils (purple). Platelets (green). Wall shear stress 6 dyn cm^{-2}.

Movie S19. 360-degree view of the SIM image showing the distribution of F-actin (purple) and P-selectin (blue) on platelets attached to an arrested neutrophil. SCD human (steady state) blood perfused through microfluidic micro-channels presenting P-selectin, ICAM-1 and IL-8 and fixed under flow. Wall shear stress 6 dyn cm^{-2}.

Movie S20. Neutrophils (red) and platelets (green) trafficking through the pulmonary microcirculation (purple) in a SCD mouse after 0.1 µg/kg IV LPS + anti-P-selectin mAb Fab fragments. A freely circulating neutrophil is seen trafficking up the arteriole into the capillaries. Pulmonary vaso-occlusion is absent. 2/3x original acquisition rate.

Movie S21. Disintegration of an embolic neutrophil-platelet aggregate following arrival at the pulmonary arteriolar bottle-neck in a SCD mouse administered 0.1 µg/kg IV LPS + anti-P-selectin mAb Fab fragments. Neutrophil (red). Platelets (green). Pulmonary microcirculation (purple). 2/3x original acquisition rate.